Modelling Flame Response of a Co-axial LOx/GH2 Injection Element to High Frequency Acoustic Forcing

Scott Beinke[1, 2], Federica Tonti[1†], Sebastian Karl[3], Justin Hardi[1], Michael Oschwald[1], and Bassam Dally[2]
[1]*German Aerospace Center (DLR)*
Institute of Space Propulsion
Lampoldshausen, D-74239 Hardthausen, Germany
[2]*The University of Adelaide*
School of Mechanical Engineering
Adelaide 5005, South Australia, Australia
[3]*German Aerospace Center (DLR)*
Institute for Aerodynamics and Flow Technology
Göttingen, 37073 Göttingen, Germany

scott.beinke@dlr.de · federica.tonti@dlr.de
[†]Corresponding author

Abstract

In the current work a URANS model of a single injection element is employed to study the response of a single coaxial LOx/GH2 injection element to an imposed acoustic disturbance representative of high frequency combustion instabilities. The model is representative of a combustion instability experiment, dubbed BKH, operated at the DLR Institute of Space Propulsion. In this study the response to uniform acoustic pressure and transverse acoustic velocity forcing is investigated. The model results are compared with optical data from BKH experiments and are shown to reproduce the deformation of the LOx core under acoustic excitation.

1. Introduction

High frequency combustion instability is not yet fully understood and cannot be predicted; increasing risk and necessitating extensive ground testing to verify the safe operation of new rocket combustor designs and configurations. High frequency combustion instability research focuses on identifying the coupling mechanisms that occur between acoustic and combustion processes which may lead to instabilities. Understanding how a flame responds to an acoustic disturbance in order to support the instability is therefore of primary interest.

Experimental research combustors have been employed to investigate combustion instability phenomena. These experiments subject injection elements to representative acoustic disturbances and observe the flame response. The combustion instability experiments feature specialised diagnostics and instrumentation to observe the flame response to either natural or externally imposed disturbances. However the diagnostics are limited and experimental datasets provide only limited insight into the underlying phenomena. Data from the experiments are also used to validate combustion instability models. The models may then allow further insight into the experiments themselves and may eventually be used to predict the flame response and combustion instability phenomena.

This work focuses on a high frequency combustion instability experiment, designated BKH, operated at the DLR Institute of Space Propulsion. BKH optical data is analysed to identify the flame response to longitudinal and transverse acoustic excitation and to produce results for numerical validation. An unsteady model of a single BKH injection element subjected to a representative acoustic disturbance is also presented. The results of the single injector model are compared with the experimental data to demonstrate that the model reproduces the experimentally observed flame response. The model is then employed to investigate the flame response over a range of excitation amplitudes.

In this paper a brief background of BKH is first provided. Results from analysis of BKH optical data are also presented. The single injector model is then described and results are presented for both acoustic pressure and transverse acoustic velocity forcing. The results of the single injector model are compared with the results from the experimental optical data analysis.
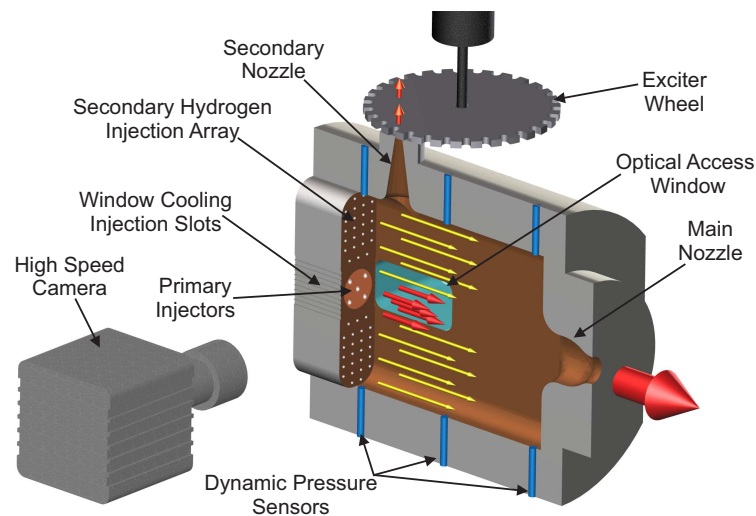
Figure 1: Concept diagram of the BKH combustor

2. Experimental Setup

BKH operates at pressures ranging from 40 bar (sub-critical oxygen pressure) to 60 bar (super-critical oxygen pressure) using cryogenic liquid oxygen (LOx) and hydrogen (H_2) propellants. The combustion chamber features a rectangular geometry with windows located on each side for optical access to the near injector region, and a secondary nozzle and toothed wheel excitation system. The combustion chamber volume is 240 mm long, 50 mm wide and 200 mm high, not including the main and secondary nozzles. A series of five coaxial study elements are positioned in a matrix pattern in the middle of the chamber. Figure 1 depicts the configuration of BKH experiments.

During operation the toothed wheel is rotated at a controlled speed in order to periodically interrupt the flow through the secondary nozzle. The periodic interruption of flow causes an acoustic disturbance to propagate back into the chamber. The frequency of the disturbance is controlled by the rotational speed of the wheel. The rectangular shaped internal volume was designed to deliberately fix the orientation of the transverse acoustic mode and to ensure the resonant mode frequencies of the chamber volume match those of full-scale upper-stage rocket engines. Dynamic pressure measurements are recorded at various locations on the combustion chamber walls to resolve the acoustic field. Methods for reconstructing the acoustic field from the dynamic pressure sensor data have been previously described in [5, 6].

Each resonant mode has a different orientation and distribution which produces a different disturbance around the primary injection elements. By controlling which mode is excited using the excitation system the response of the flame to different acoustic disturbances can be observed. When the first longitudinal mode is excited, the primary injection elements lie in a pressure antinode. Similarly during transverse mode excitation the injection elements lie near a pressure nodal line and are subjected to acoustic velocity fluctuations. The response of the injection elements to the acoustic disturbance is observed via simultaneous high-speed shadowgraph and OH chemiluminescence (OH*) imaging captured through the optical access windows in the side walls of the chamber.

BKH experiments are conducted at the European Research and Technology test Facility P8 for cryogenic rocket engines at DLR Lampoldshausen. Additional information on BKH can be found in [13, 14, 16, 17]. The work presented here focuses on results for a single BKH operating point with a chamber pressure of 60 bar and a oxidizer to fuel ratio (ROF) of 6 for the primary BKH injection elements, commonly referred to as the 60 bar ROF 6 operating point. This operating point is referred to as supercritical as the chamber pressure is greater than the critical pressure of both the injected oxygen and hydrogen propellants.

2.1 Optical Diagnostics

The optical diagnostics setup employed during BKH experiments is shown in Figure 2. To allow simultaneous imaging a dichroic mirror positioned at 45° to the optical axis is used to reflect ultra-violet light to the OH-imaging camera without interrupting the optical path between the back-lighting source and shadowgraph imaging camera. The optical setup employed during the BKH experiments has been previously described by Hardi [13, 15, 16].
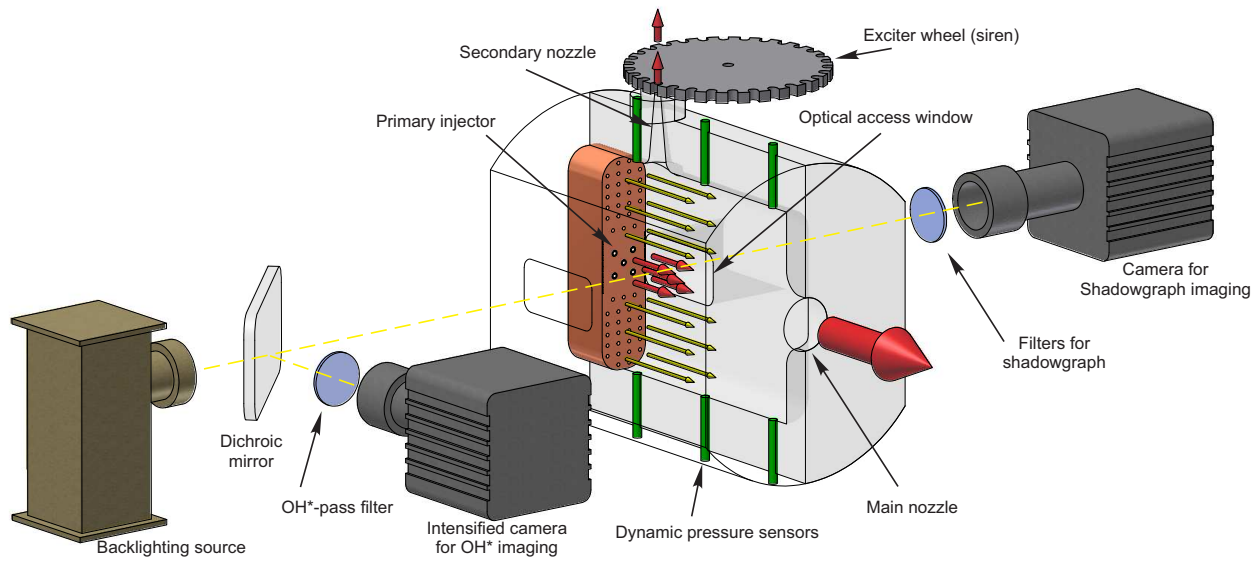
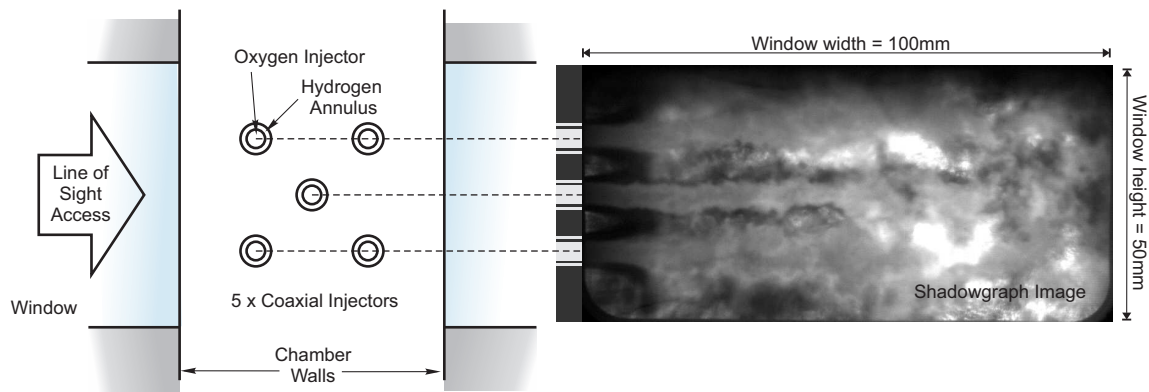Figure 2: BKH optical diagnostics setup [16].

Figure 3: Visualisation of line-of-sight access in BKH and a shadowgraph image recorded without acoustic excitation.

High speed shadowgraph images have been collected at the 60 bar ROF 6 operating point. The shadowgraph images were captuded using a RG850 longpass optical filter to block wavelengths shorter than 850 nm in order to suppress combustion light but not the powerful near-infra-red light emitted by a Xenon lamp used as the back-lighting source. Line-of-sight images are recorded through the windows in side walls of the chamber as shown in Figure 3. Due to the penta-injector configuration, two of the five injection elements are hidden behind other elements and only 3 distinct jets are visible in the images.

3. Experimental Data Analysis

A samples shadowgraph image is shown in Figure 3. This sample is from a test period when the excitation frequency does not match a resonant mode of the combustor volume. Previous works by Hardi et al. [13, 14, 16, 17] have presented BKH optical datasets and analysis describing the deformation of the flame during transverse and longitudinal excitation. More recent work [6] applied dynamic mode decomposition (DMD) analysis to isolate and identify new features in the BKH images. This work has since been applied to additional BKH optical datasets in which new features have been identified.

Figure 4 shows instantaneous and time-averaged shadowgraph images from a optical dataset captured during 1L-mode excitation in which the primary injection region is located within a pressure antinode. The camera was focused on a small region near the injection plane and the LOx core of the central injector occupies the lower portion of the image. This region was chosen in order to visualise the interface between the oxygen and hydrogen streams. Fluctuations on the surface of the LOx jet can be seen in the instantaneous image which are not present in the time-averaged image.
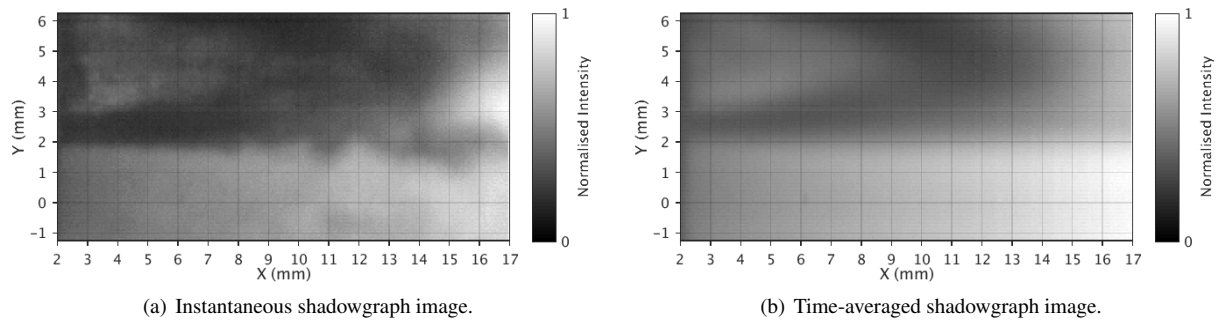
(a) Instantaneous shadowgraph image.

(b) Time-averaged shadowgraph image.

Figure 4: Samples of instantaneous and time-averaged optical images from BKH test during 1L-mode excitation [33].

(a) Reconstructed image.

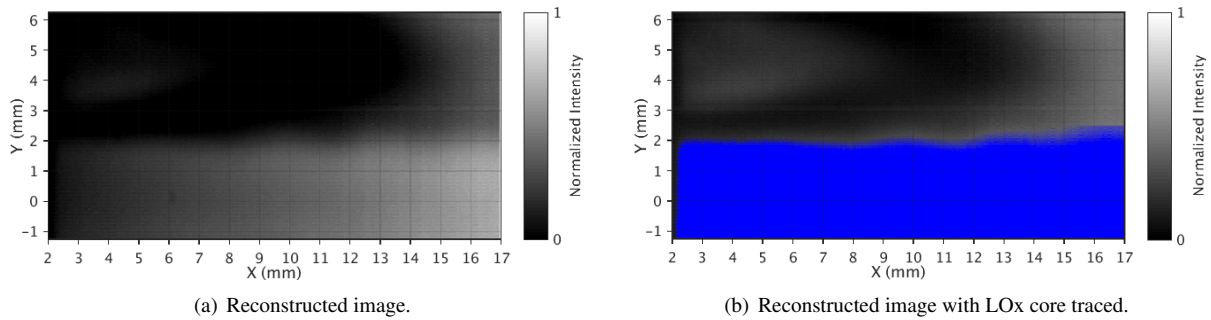(b) Reconstructed image with LOx core traced.

Figure 5: Reconstructed optical images from DMD analysis of shadowgraph images captured during 1L-mode excitation.

DMD analysis of the 1L optical sample was used to identify coherent structures and motion at the excitation frequency. The identified fluctuations at the excitation frequency were then used to produce a sequence of reconstructed DMD images. An "instantaneous" image reconstructed from the mean image and the DMD modes at an particular instant is shown in Figure 5(a). Figure 5(b) shows the reconstructed image with the LOx core traced in blue. The reconstructed images show wave-like fluctuations on the surface of the LOx core. These wave-like structures are periodic and their spacing is related to the excitation frequency.

Figure 6 shows instantaneous and time-averaged shadowgraph images from an optical dataset captured during 1T mode excitation. The camera captures the extent of the flame within the entire window region. During 1T-mode excitation the pressure nodal line passes through the primary injection region and the primary injection elements are subjected to transverse velocity fluctuations. The acoustic motion also increases mixing of the oxidiser and fuel streams which accelerates the breakup of the dense LOx core. The length of the flame is observed to shorten and retract towards the faceplate during 1T mode excitation as seen in Figure 6.

Figure 7 shows reconstructed instantaneous images from the DMD analysis of the 1T shadowgraph optical data. Figure 7(a) shows a reconstructed image of the entire window region, while Figure 7(b) shows a zoomed-in view of the LOx core from the central injection element which has been traced in blue. The images show the retraction of the flame, but also the presence of wave-like structures near the injection plane that alternate between the top and bottom surface of the LOx core. These surface structures become less pronounced further downstream near the end of the liquid core. Over a sequence of images the downstream part of the core is observed to be periodically transported vertically by the transverse acoustic velocity acting across the primary injection elements.

The DMD analysis has been used to identify the mean deformation of the LOx core under continuous acoustic excitation. The identified phenomena will be compared with the results of the numerical model described in the following sections.

4. Numerical Method

Initial modelling of BKH experiments has focused on models of single injection elements subjected to a representative acoustic disturbance [5, 6]. This approach has now been applied to investigate the flame response over a range of excitation amplitudes and to both longitudinal and transverse acoustic excitation. Unsteady RANS computations are computed to model single injection elements using a specialised implementation of the DLR TAU code with real-gas modelling capability. During the unsteady computation the boundary conditions of the domain are modified to impose an acoustic disturbance representative of the local acoustic fluctuations. The DLR Tau code and the single injector models are described in more detail in the following sections.
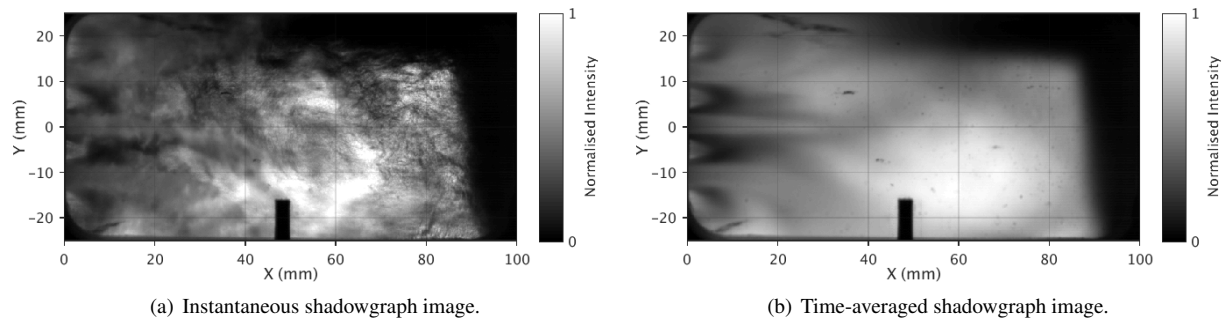
(a) Instantaneous shadowgraph image.

(b) Time-averaged shadowgraph image.

Figure 6: Samples of instantaneous and time-averaged optical images from BKH test during 1T-mode excitation [16].

(a) Reconstructed image.

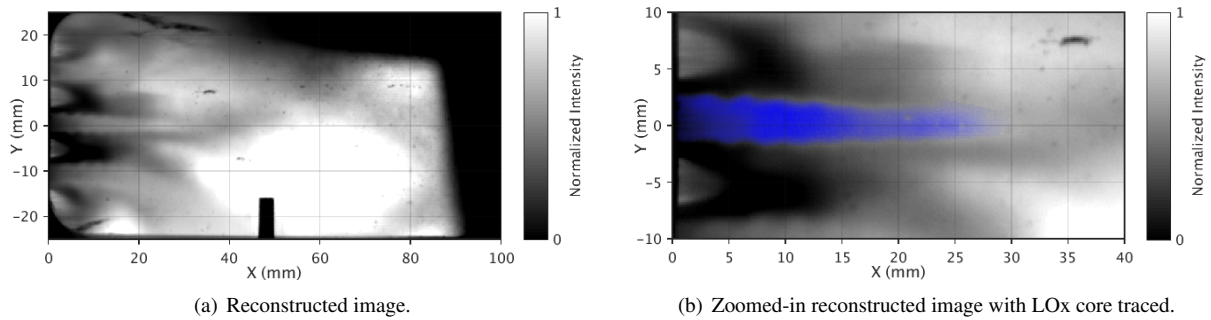(b) Zoomed-in reconstructed image with LOx core traced.

Figure 7: Reconstructed shadowgraph images from DMD results from BKH 1T-mode excitation optical dataset.

4.1 CFD Solver

The DLR TAU code is a hybrid (structured/unstructured) grid Godunov-type finite-volume flow solver for the compressible Euler and Navier-Stokes equations. Spatial second order is reached by a MUSCL reconstruction. The DLR TAU code has been validated for a range of steady and unsteady flow cases [9, 21, 28, 29] and is further described in [12, 18, 29].

The one-equation Spalart-Allmaras [31] turbulence model was selected for the current work due to its simplicity and ease of implementation. This turbulence model yields satisfactory results for a wide range of applications while being numerically robust and computationally inexpensive. A MAPS+ Riemann solver by Rossow [26] is also used to handle the low Mach number flows and high density gradients which are a challenge to a compressible flow solver.

An explicit 3$^{\text{rd}}$ order Runge-Kutta scheme was used for time integration. To perform unsteady computations a Jameson-type dual time stepping scheme with a physical time step size of 5.0×10^{-6} s and 1000 inner iterations per physical time step was used.

A finite rate chemistry scheme that solves the Arrhenius equation is used in the current work. A six-species and seven-step reaction scheme for oxygen-hydrogen combustion published by Gaffney et al. [8] that includes the species H_2, O_2, H, O, OH, and H_2O was employed.

Cryogenic propellants at high pressures, as encountered in rocket engines, behaves differently than ideal gases. To account for these real-gas effects a specialised release of the TAU code [4] is employed to model injection and combustion of cryogenic propellants. Banuti [2, 4] explains that this specialised real gas implementation has two distinct features: A dedicated equation of state is used for each species, and a multi-fluid mixing model is used to determine the properties of the mixture. The model, and its validation, are described in more depth by Banuti[2, 3].

The dedicated equation of state allows a higher fidelity but computationally expensive equation of state to be used for propellants that must be considered as real-gases, and a more efficient equation of state for other species. Here, an ideal gas equation is solved for each of the species H_2, OH, H_2O, O, H, and a real-gas equation of state is used for O_2. The real gas properties of oxygen are computed from the high fidelity modified Benedict-Webb-Rubin (MBWR) equation of state (EOS) of Younglove [34] and stored in a library during a pre-processing step. Thermodynamic state variables, such as pressure, enthalpy, heat capacities, speed of sound, etc. are all computed consistently from the real gas EOS. Real gas corrections to the transport coefficients are evaluated following Lemmon and Jacobsen [20].

The currently implemented multi-fluid mixing model assumes ideal mixing of species properties. This is only valid if all species exist as a real-gas in only a pure-fluid state. However this assumption is physically justified in this work focused on supercritical oxygen-hydrogen combustion. Numerical studies by Oefelein [22, 23] have noted the flame produced by a coaxial injection element in an oxygen-hydrogen liquid propellant rocket engine effectively
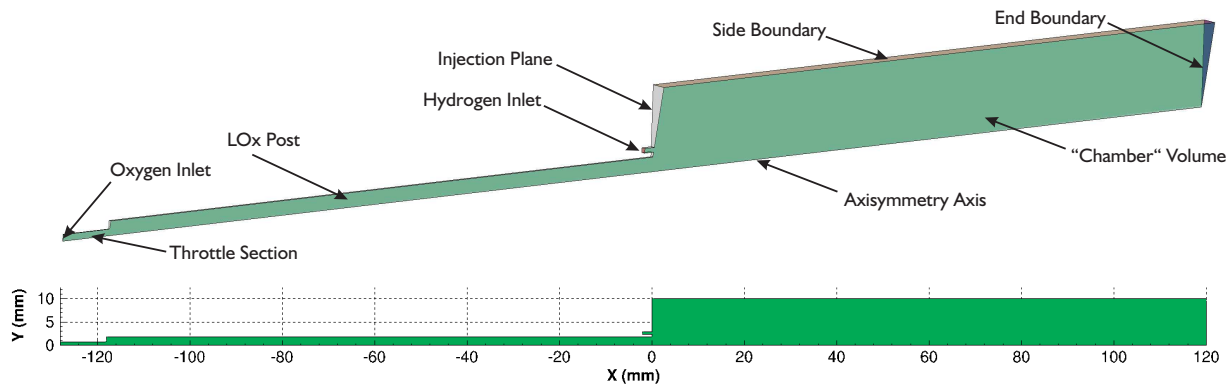
Figure 8: Domain used for 2D axisymmetric single injector computations.

isolates the fuel and oxidiser streams. This agrees with similar experimental observations made by Oschwald et al. [24] and many others. Numerical studies of representative reactive cryogenic shear layers [7] by Bellan and 1D counterdiffusion flames by Ribert et al. [25] and Lacaze et al. [19] have shown that mixing in the hot reaction zone occurs under ideal gas conditions.

Banuti et al. [1, 4] further explain that, for oxygen-hydrogen combustion at supercritical pressures, the LOx transitions from a liquid-like to a gaseous state under pure fluid conditions, where essentially all real fluid effects are confined to the LOx core. Thus for the flames considered in the present work, the multi-fluid ideal-mixing model is appropriate. The fluid in the numerical domain is assumed to exist as either a pure-fluid real-gas or a mixture that can be approximated using an ideal-mixing model. The fluid is treated as a continuous Eulerian mixture with no discrete phases or phase changes. This approach is sometimes referred to as an Euler-Euler model.

4.2 Domain and Boundary Conditions

Two different domains were used to study pressure and velocity excitation of a BKH coaxial injection element. Both domains modelled part of the injector geometry connected to a larger volume representing part of the chamber volume. A 2D axisymmetric domain was used for modelling a BKH injector subjected to acoustic pressure forcing. The axisymmetric domain was chosen as the pressure fluctuations were to be imposed symmetrically about the flame as if it were in a pressure anti-node and velocity node. The axisymmetric disturbance does not disturb the flame from the centreline of the injector and it can therefore be approximated with a 2D axisymmetric domain. The 2D axisymmetric domain is shown in Figure 8.

The LOx post geometry is included in the 2D axisymmetric model to investigate the possibility of LOx post coupling. LOx post coupling has been identified as a possible instability mechanism experimentally by Gröning et al. [10] and numerically by Urbano et al. [32] while investigating a naturally unstable oxygen-hydrogen combustion instability experiment.

The small volume downstream from the injection plane is chosen to capture the extent of the flame as it propagates into the larger chamber volume. The chamber volume in the 2D axisymmetric model is 120 mm long and has a radius of 10 mm. The length of the domain was chosen to be slightly longer than the 100 mm length accessible via optical access in BKH. The 10 mm radius was chosen for the current work as it produces a representative flame distribution which contains the flame within the numerical domain during acoustic excitation. However the single injector domain does not capture the influence of the surrounding elements in the penta-injector configuration used in BKH.

To investigate the flame response to transverse acoustic velocity forcing a 3D numerical domain was employed which is shown in Figure 9. The 3D domain was necessary to capture both the vertical transport and horizontal flattening of the flame during transverse excitation. In the current work the single injector model is subjected to a one-dimensional transverse disturbance. A symmetry condition is prescribed in the plane parallel to the imposed disturbance and injection velocity. This symmetry plane allowed the numerical domain to be reduced to include only one half of the injector and flame while still capturing the relevant phenomena.

As the hydrogen and oxygen injectors reside in a pressure node during transverse excitation limited coupling with the injection elements is expected to occur. Therefore the oxygen and hydrogen posts are not included in the 3D numerical domain. Instead only a short section of both the oxygen and hydrogen injectors before the injection plane is included.
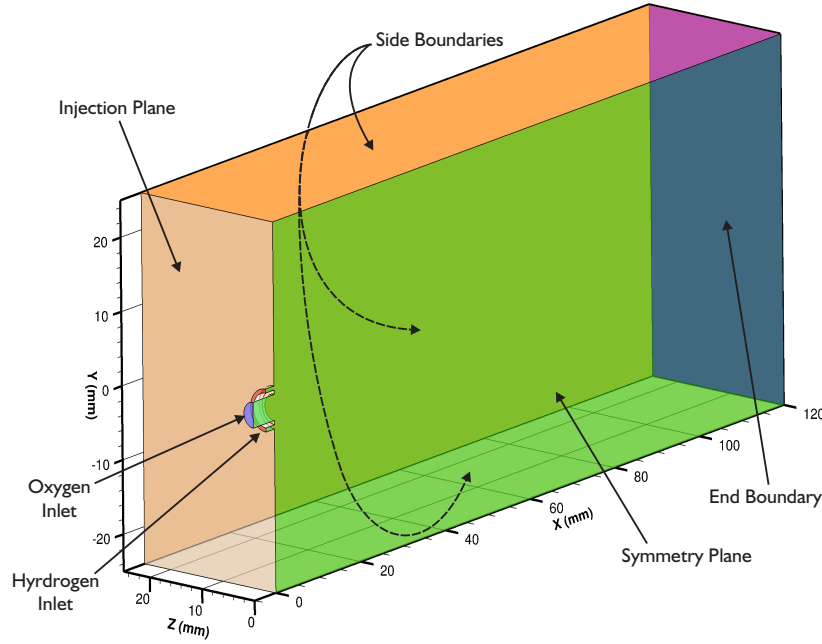
6

Figure 9: Domain used for 3D single injector computations.

The downstream volume attached to the injection plane is again used to represent a local region of the internal chamber volume and extends 120 mm from the injection plane. The cross-section is 25 mm wide by 50 mm high which, with the symmetry plane, is equivalent to a 50 mm by 50 mm box enclosing a single BKH injection element. The dimensions of the 3D numerical domain were chosen in order to contain the flame from the single injection element while being sufficiently large that the flame does not intersect the side boundaries during transverse excitation.

Similar boundary conditions are prescribed for both the 2D and 3D single injector models. Mass flow rate boundary conditions are specified at the oxygen and hydrogen inlet boundaries to match the 60 bar ROF 6 operating point reached during BKH experiments. The post walls, post tip, and injection plane are specified as adiabatic viscous walls. To compute an initial steady-state RANS solution the side boundaries of the "chamber" volume are specified as an inviscid wall and a farfield condition is prescribed at the end boundary of the domain. The farfield boundary state is specified by defining the composition, density, velocity, and temperature of a mixture. During the RANS computation the flow across the boundary is determined based on the difference between the internal flow state and the boundary farfield state. The state at the farfield boundary is therefore used to control the pressure in the numerical domain and is specified as an equilibrium mixture of combustion products at the desired chamber pressure. The equilibrium mixture prescribed at the farfield boundary is computed using the oxygen and hydrogen flow rates through the injector and consists predominantly of hydrogen and water.

For unsteady computations the side and end boundaries of the chamber domain are specified as farfield boundary conditions. The state of the farfield boundary condition is modified at each physical time step during the unsteady computation in order to impose the desired acoustic disturbance. The disturbance is imposed as a dynamic fluctuation about the steady-state solution:

$$p = \bar{p} + p' \tag{1}$$

where p is the imposed pressure, $\bar{p}$ is the steady-state pressure distribution, and p' is the dynamic acoustic disturbance.

The farfield boundary is used to represent an internal fluid boundary rather than a physical wall. As the local internal flowfield state adapts to the specified farfield distribution the acoustic disturbance is imposed upon the numerical domain.

This method for imposing acoustic excitation was originally chosen due to the relative ease of implementation with existing numerical tools. However, there are a number of consequences to this approach. The mass entering the domain across the boundary has the specified mixture properties of the farfield boundary. In this work the farfield boundary species distribution is adapted from the steady-state solution so that mass entering the domain has the same mixture composition as the steady state solution. Therefore a significant limitation of the current approach is that the flow entering the domain during the pressure peak of the acoustic cycle is not the same as the flow leaving the domain during the low pressure part of the acoustic cycle.
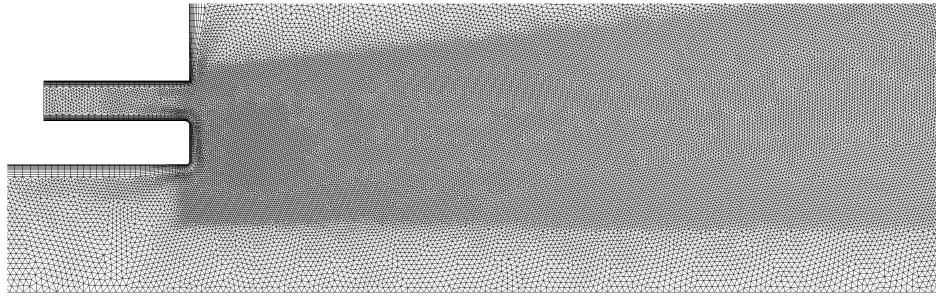
Figure 10: Near injector region of 2D axisymmetric mesh used for acoustic pressure excitation computations.
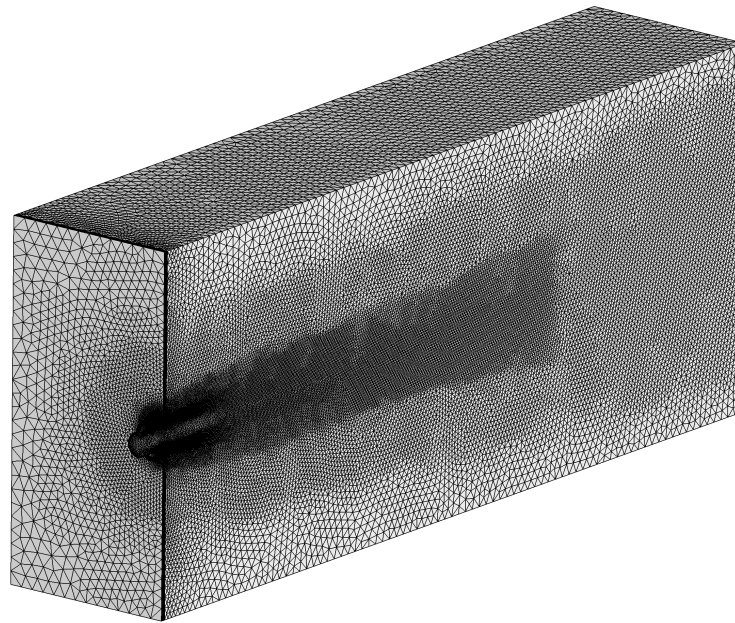

Figure 11: Mesh used for 3D transverse acoustic velocity computations.

The single injector model is therefore more representative of a single isolated element in a chamber full of combustion products. As most of the heat release occurs near the injection plane and the dimensions of the domain have been chosen to ensure the flame does not come into direct contact with the side and end boundaries this limitation is believed to have only a minor impact on the results. However the influence of the neighbouring jets in the experimental penta-injector configuration are also ignored in the 3D single injector model.

Unstructured meshes of the 2D and 3D numerical domains were used for the unsteady computations. Both of the meshes were refined near the LOx post tip, in the region occupied by the LOx core, and in the shear layer between the oxygen and hydrogen propellant streams. Prismatic boundary layers were prescribed at viscous boundary surfaces while the rest of the numerical domain was filled with tetrahedral elements. The unstructured mesh of the 2D domain contained approximately 160,000 nodes. The axisymmetric mesh in the region near the injection plane is shown in Figure 10. The size of mesh elements varied from a minimum size of 0.03 mm in the shear layer, to a maximum element size of 0.5 mm downstream.

The mesh used for the 3D velocity computations is shown in Figure 11. The unstructured 3D mesh used approximately 590,000 nodes to fill the half injector domain. The mesh was locally refined in the center of the domain to resolve the shear layer and LOx core. The smallest element size was 0.08 mm in the shear layer at the post tip. A stretching factor of 1.2 was defined to increase the size of the mesh away from the central combustion region with the largest elements having a size of 2 mm at the outer side and end boundaries of the domain. The mesh used for the 3D computations was signficantly coarser than that used for the 2D axisymmetric computations. This was primarily due to the 2D computations being relatively inexpensive which facilitated a more refined mesh.

5. Numerical Results

The results of new single injector model studies using the DLR TAU code are presented in this section. Each model was initialised by first computing a steady-state solution representing the unexcited flame. The response of the single injector to an imposed acoustic disturbance was then modelled by subjecting the steady-state solution to a representative disturbance by modulating the side and end boundary conditions during an unsteady computation. While the amplitude of the disturbance is difficult to control experimentally, the disturbance applied numerically can be readily controlled and the models have been used to investigate the flame response over a range of excitation amplitudes.

5.1 Acoustic Pressure Forcing

The 2D axisymmetric model of a BKH injection element was subjected to a uniform acoustic pressure fluctuation. The acoustic pressure fluctuation is representative of the local acoustic disturbance acting upon the flame in BKH experiments during 1L-mode excitation. The excitation system in BKH is optimized for exciting the transverse modes and so the amplitude of the longitudinal mode reached experimentally is quite low (< 3% chamber pressure). The flame response to higher amplitude disturbances has been investigated using the single injector model.
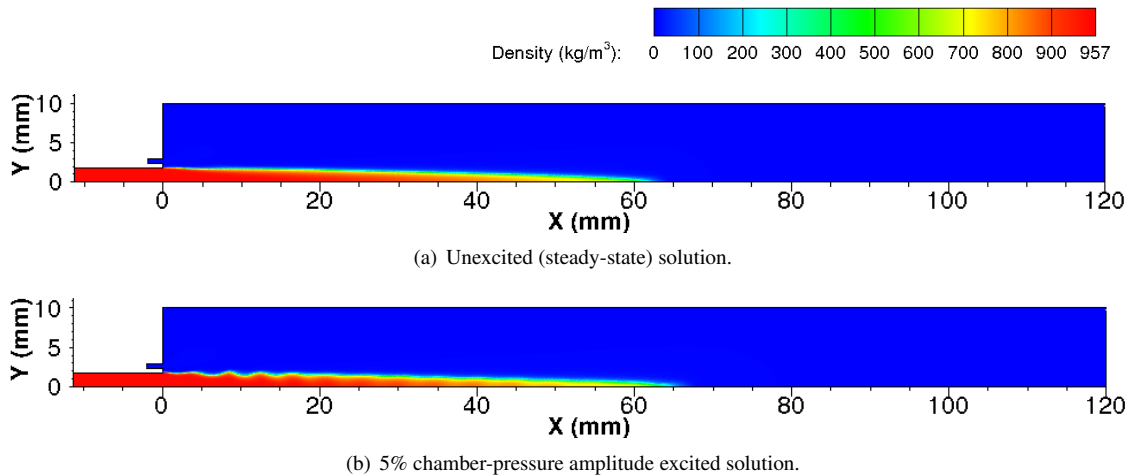

(a) Unexcited (steady-state) solution.

(b) 5% chamber-pressure amplitude excited solution.

Figure 12: Density distribution in single injector volume with and without acoustic pressure forcing.

(a) Unexcited (steady-state) solution.
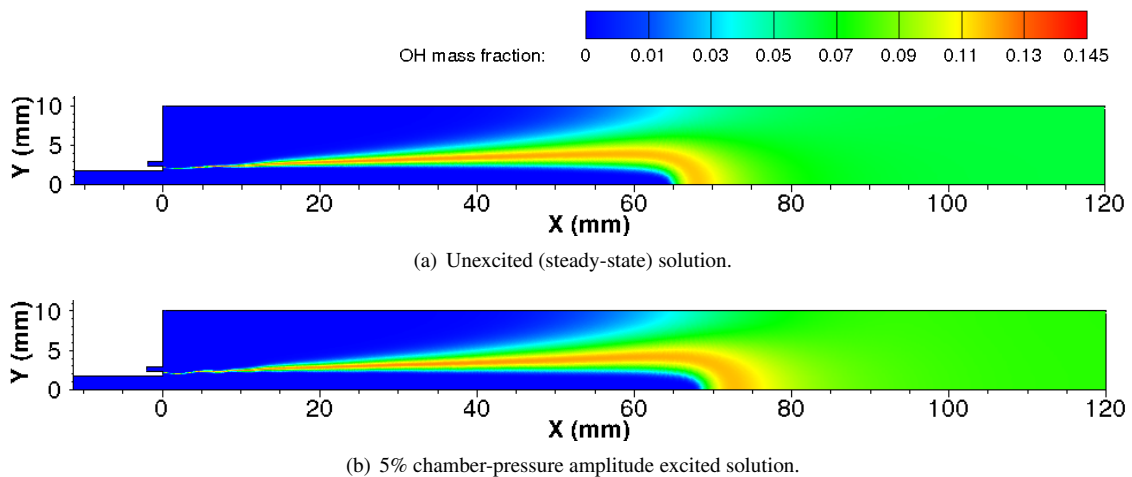

(b) 5% chamber-pressure amplitude excited solution.

Figure 13: OH distribution in single injector volume with and without acoustic pressure forcing.

MODELLING FLAME RESPONSE OF A COAXIAL LOX/GH2 ELEMENT TO HIGH FREQUENCY ACOUSTIC FORCING

(a) Phase = 0

(b) Phase = π

Figure 14: Reconstructed images at different phases of the acoustic cycle from DMD analysis of zoomed-in shadow-graph images capturing surface of LOx core. LOx core highlighted in blue.
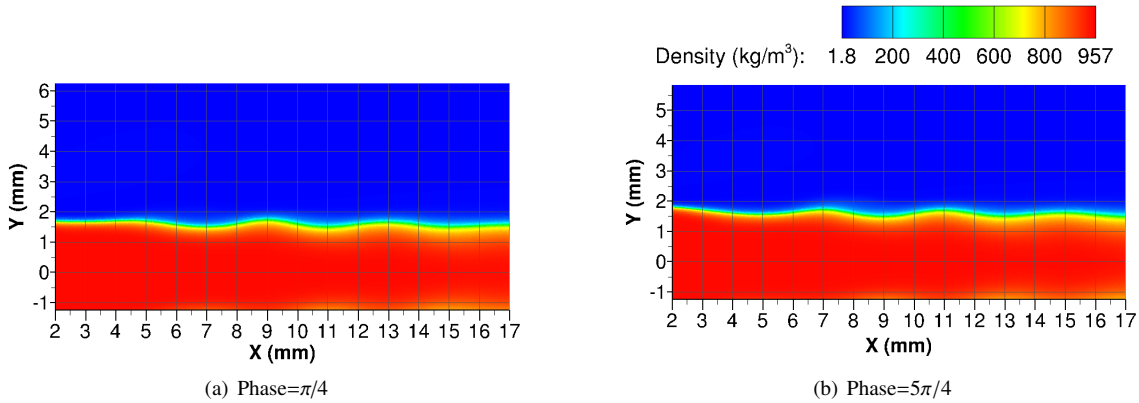

(a) Phase=π/4

(b) Phase=5π/4

Figure 15: Density distribution at same location Test C 1L shadowgraph images at different phases of the acoustic cycle for 1.5 bar pressure amplitude computation.

Figures 12 and 13 show the change in density and OH mass fraction distributions relative to the unexcited solution from a computation with an acoustic amplitude equivalent to 5% of the combustion chamber pressure. The acoustic pressure fluctuation cause wave-like structures to form on the surface of the dense LOx core near the injection plane. These structures propagate downstream and become less distinguished as the density of the LOx core decreases downstream. The OH mass-fraction distribution indicates the location of the flame. While the length of the flame increases slightly once acoustic excitation is imposed, the flame is otherwise not significantly altered. The increased length may be due to the excitation boundary conditions producing a slight velocity variation along the length of the domain.

The wave-like deformation of the LOx core predicted numerically is compared with the previously identified structures in the reconstructed DMD results in Figure 14. The experimental data is captured from a period where the excitation amplitude is equivalent to 2.5% of the chamber pressure so the experimental data are compared with the results from a computation with a similar excitation amplitude. The numerical results shown in Figure 15 exhibit the same propogation of wave-like structures on the surface of the dense LOx core as observed experimentally. The numerical model also show a similar position and spacing between the wave-like structures. Further quantitative comparison is difficult due to the uncertainty of the experimental optical data.

The instantaneous density distribution predicted by the numerical model with different acoustic excitation amplitudes is shown in Figure 16. These results show that the wave-like structures become more pronounced at higher excitation amplitudes. These results will be analysed further in future work to characterise the flame response.

5.2 Transverse Acoustic Velocity Forcing

The response of BKH injection elements to a transverse acoustic velocity disturbance, representative of the local acoustic disturbance acting upon the flame during 1T-mode excitation of BKH experiments, has been investigated numerically using the single injector model. As acoustic excitation is imposed the increased mixing and introduction of fresh propellant species to the combustion zone accelerate the consumption of the LOx core. As the LOx core is consumed the flame similarly retracts towards the injection plane.

(a) 2.5% chamber-pressure amplitude

(b) 5% chamber-pressure amplitude

(c) 7.5% chamber-pressure amplitude
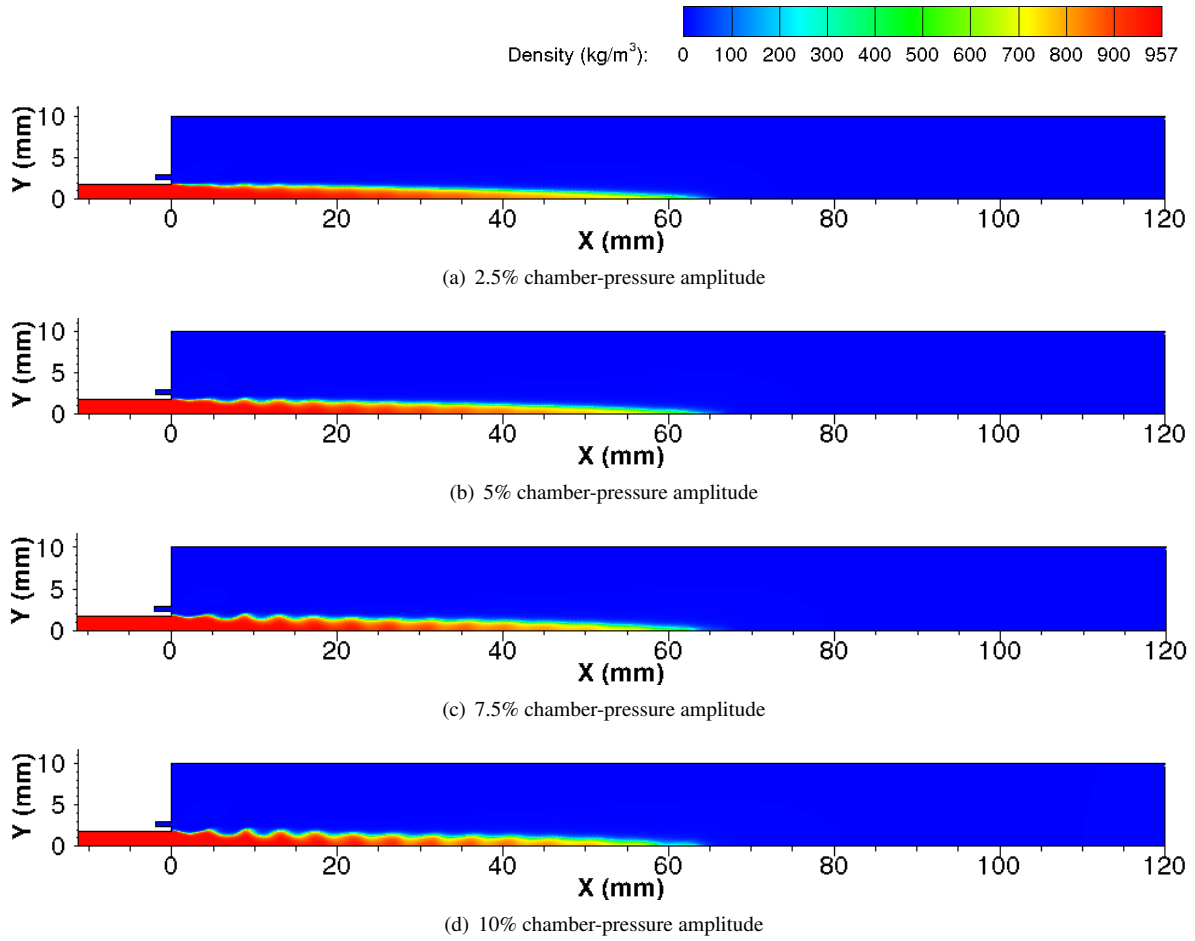
(d) 10% chamber-pressure amplitude

Figure 16: Comparison of density distribution in chamber volume resulting from acoustic pressure excitation with different excitation amplitudes.

Previous work [5, 6] presented initial results and described the retraction, flattening, and motion of the LOx core and flame under continuous acoustic excitation. This work has been repeated to investigate the flame response to a range of acoustic excitation amplitudes.

The primary result for experimental comparison is the deformation and length of the LOx core after acoustic excitation has been applied. Figure 17(a) shows an image from the previously discussed DMD analysis of shadowgraph data. The zoomed-in view of the reconstructed image shows the LOx core from the central injection element which has been highlighted in blue. Figures 17(b) and 17(c) show comparable results indicating the distribution of the dense LOx from a single injector model subjected to a similar amplitude acoustic velocity disturbance. The single injector model has reproduced both the retraction of the flame, and the alternating wave-like surface structures on the surface of the LOx core near the injection plane.

Hardi et al. [13, 15, 16] have previously analysed BKH shadowgraph data and identified a trend of exponential decay of the length of the LOx core with increasing excitation amplitude. The same trend has been reproduced by the single injector model at different excitation amplitudes, as shown in Figure 18. Figure 18 also shows that the numerically predicted LOx core length is significantly shorter than that observed experimentally. This difference is attributed primarily to the assumptions of the single injector model. In particular how the single injector domain does not capture the influence of neighbouring injection elements which would shield or protect the central injection element from the acoustic velocity. The domain also does not capture the acceleration of the flow along the length of the chamber which would affect the length of the flame.

6. Discussion

The single injector model subjected to a representative acoustic disturbance has reproduced the wave-like surface fluctuations on the LOx core identified experimentally during both 1L and 1T mode excitation. The additional cases computed with higher excitation amplitudes than can be reached experimentally indicate that this effect becomes more

MODELLING FLAME RESPONSE OF A COAXIAL LOX/GH2 ELEMENT TO HIGH FREQUENCY ACOUSTIC FORCING

(a) Image reconstructed from DMD analysis. LOx core highlighted in blue.

(b) Density isosurfaces shown at 10 and 50 kg/m^3.

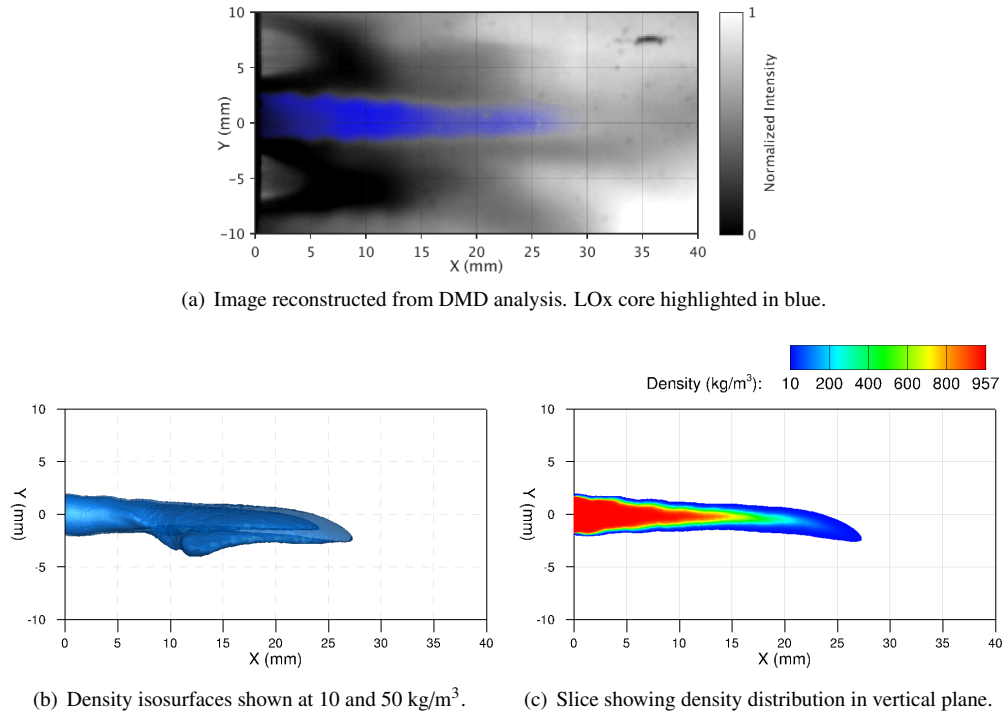(c) Slice showing density distribution in vertical plane.

Figure 17: Comparison of experimental and numerical LOx core surface fluctuations for an excitation amplitude of 7.1% chamber pressure. Density shown with a cut-off value of 10 kg/m^3.
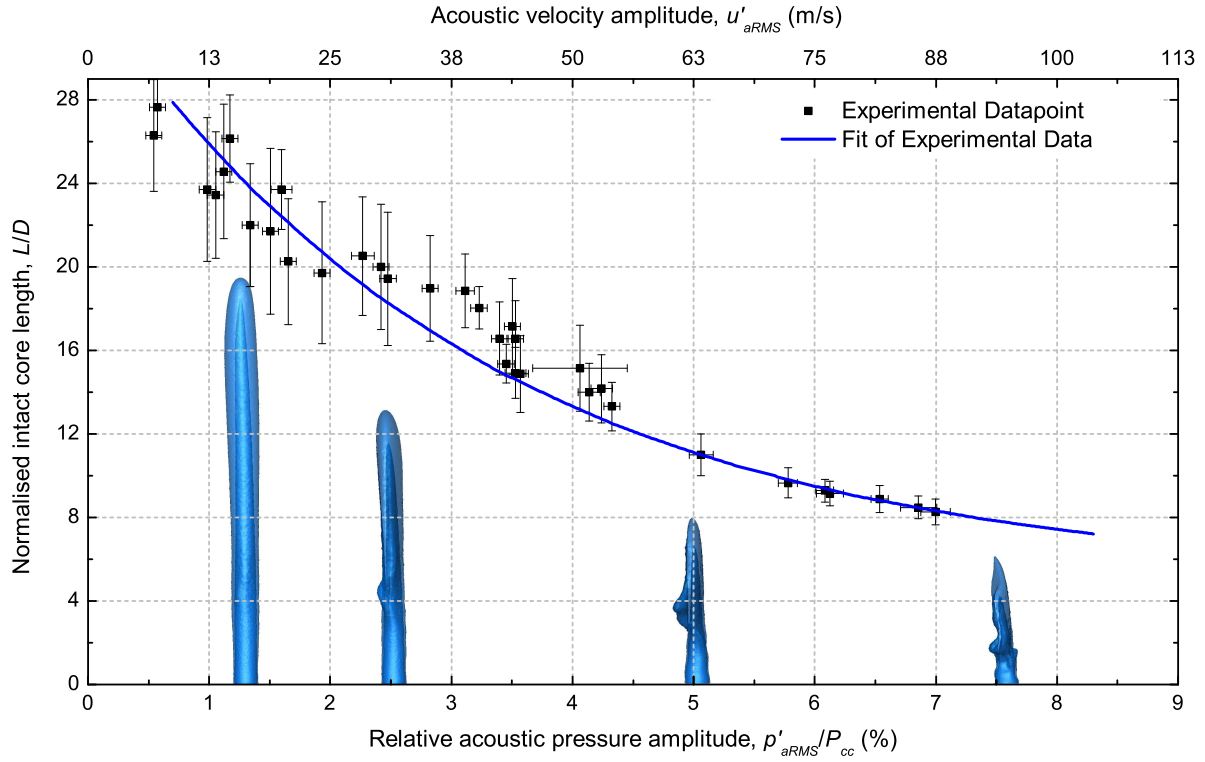

Figure 18: Experimental and numerical results showing LOx core length versus transverse mode amplitude. Experimental data from Hardi et al. [13]. Numerical results shown as side view of blue density isosurfaces at density values of 10 and 100 kg/m^3.

pronounced as the disturbance amplitude increases. The wave-like structures are attributed to the different response of the oxygen and hydrogen propellant streams to the imposed acoustic disturbance. This difference produces a fluctuation of the relative injection velocity. The acoustics of the injection system and in particular the LOx post may also contribute to this fluctuation. The further analysis of the model results will be used to investigate this phenomena. These results will also allow better interpretation of experimental results in future work.

Improved modelling of transport coefficients to the real-gas TAU implementation as compared to the results presented in [5, 6] have corrected previously identified issues related to the thermal conductivity of the dense gas. Therefore the thermal-breakup of the dense oxygen jet, which was previously over-predicted, has been improved in recent work. This modification indicates the usefulness of the experimental optical data for numerical validation, as previous results with higher thermal conductivity did not capture the fine wave-like fluctuations on the surface of the dense LOx core. These features have been reproduced in the current work and this result increases the level of confidence in the model results.

While the model has qualitatively reproduced the trend of exponential decay with increasing excitation amplitude, further quantitative comparison is difficult. The image intensity captured in shadowgraph images cannot be related to a specific density value. Similarly, the density distribution is not quantitatively comparable to the emission captured in the shadowgraph images. Further understanding of the radiation captured in shadowgraph images, and suitable post-processing methods to produce quantitatively comparable line-of-sight images from numerical data are needed before a quantitative comparison can be made.

The flattening, flapping, and retraction of the liquid oxidiser core from a coaxial injection element under transverse acoustic excitation has previously been identified using LES[11, 30] and URANS modelling[27]. This work has demonstrated that the same phenomena can be reproduced with employed numerical approach. The single injector models can be used to compute numerical test-cases to investigate the flame response at additional operating points or conditions that cannot be reached experimentally. Once further validated the modelling approach may be applied to investigate more complicated configurations and systems.

7. Conclusion & Outlook

The experimental and numerical analyses presented in this paper has identified phenomena important for understanding the flame response of coaxial oxygen-hydrogen injection elements subjected to longitudinal and transverse acoustic forcing. This work has built upon earlier research by identifying new features for numerical comparison and by investigating the flame response over a range of disturbance amplitudes.

Wave-like surface fluctuations were identified experimentally during longitudinal and transverse velocity excitation. These fluctuations were reproduced numerically by subjecting a single injector model to a representative acoustic disturbance. The increased retraction of the flame with increasing transverse acoustic velocity excitation amplitude was also reproduced numerically. These results indicate that the simplified modelling approach employed in this work is sufficient to reproduce the experimentally observed deformation of the dense LOx core.

By modelling the flame response to acoustic excitation at multiple excitation amplitudes numerically a larger range of excitation amplitudes has been investigated than are captured experimentally. Further post-processing of the numerical results and additional testcases will be used to investigate and characterise the flame response in future work. Methods for conducting a more direct quantitative comparison and validation are needed before the numerical results before they relied upon for further analysis.

8. Acknowledgements

References

[1] D. Banuti, P.C. Ma, J.-P. Hickey, and M. Ihme. Sub- or supercritical? a flamelet analysis for high-pressure rocket propellant injection. In *52nd AIAA/SAE/ASEE Joint Propulsion Conference Salt Lake City, UT*, volume AIAA 2016-4789, 2016.

[2] Daniel Banuti. *Thermodynamic analysis and numerical modeling of supercritical injection*. PhD thesis, University of Stuttgart, 2015.

[3] Daniel Banuti and Klaus Hannemann. Efficient multiphase rocket propellant injection model with high quality equation of state. In *Proceedings of the 4th Space Propulsion Conference*, 2014.

[4] Daniel T. Banuti, Volker Hannemann, Klaus Hannemann, and Bernhard Weigand. An efficient multi-fluid-mixing model for real gas reacting flows in liquid propellant rocket engines. *Combustion and Flame*, 168:98 – 112, 2016.

[5] S. Beinke, D. Banuti, J. Hardi, M. Oschwald, and B. Dally. Modelling of a Coaxial LOx/GH2 Injection Element Under High Frequency Acoustic Disturbances. In *6th European Conference for Aeronautics and Space Sciences (EUCASS)*, Krakow, Poland, 29 June - 3 July 2015.

[6] Scott Beinke, Daniel Banuti, Justin Hardi, Michael Oschwald, and Bassam Dally. Modelling of a Co-axial LOx/GH2 Injection Element Under High Frequency Acoustic Disturbances. In *Progress in Propulsion Physics*, 2016. (In Press).

[7] Josette Bellan. Theory, modeling and analysis of turbulent supercritical mixing. *Combustion science and technology*, 178:253–281, 2006.

[8] R. L. Gaffney, J. A. White, S. S. Girirnaji, and J. P. Drummond. Modeling turbulent/chemistry interactions using assumed pdf methods. In *AIAA/SAE/ASME/ASEE Joint Propulsion Conference and Exhibit*, Nashville, TN, July 6-8 1992.

[9] T. Gerhold, O. Friedrich, J. Evans, and M. Galle. Calculation of Complex Three-Dimensional Configurations Employing the DLR-TAU-Code. *AIAA paper 97-0167*, 1997.

[10] S. Gröning, J.S. Hardi, D. Suslov, and M. Oschwald. Injector-driven combustion instabilities in a hydrogen/oxygen rocket combustor. *Journal of Propulsion and Power*, 32(3):560–573, 2016.

[11] L. Hakim, T. Schmitt, S. Ducruix, and S. Candel. Dynamics of a transcritical coaxial flame under a high-frequency transverse acoustic forcing: Influence of the modulation frequency on the flame response. *Combustion and Flame*, 162:3482–3502, 2015.

[12] V. Hannemann. Numerische simulation von stoß- stoß- wechselwirkungen unter berücksichtigung von chemischen und thermischen nichtgleichgewichtseffekten. Technical Report FB 97-07, DLR, 1997.

[13] J. Hardi, H.C. Gomez Martinez, and M. Oschwald. LOx jet atomization under transverse acoustic oscillations. *Journal of Propulsion and Power*, 30(2):337–349, 2014.

[14] J. Hardi, M. Oschwald, and B. Dally. Flame response to acoustic excitation in a rectangular rocket combustor with LOx/H2 propellants. *CEAS Space Journal*, 2:41–49, 2011.

[15] J. S. Hardi and M. Oschwald. Cryogenic oxygen jet response to transverse acoustic excitation with the first transverse and the first combined longitudinal-transverse modes. In *EUCASS Proceedings Series: Advances in AeroSpace Sciences*, volume 8, pages 75–94, 2016.

[16] Justin S. Hardi. *Experimental Investigation of High Frequency Combustion Instability in Cryogenic Oxygen-Hydrogen Rocket Engines*. PhD thesis, The University of Adelaide, 2012.

[17] Justin S. Hardi, Scott K. Beinke, Michael Oschwald, and Bassam B. Dally. Coupling of cryogenic oxygen-hydrogen flames to longitudinal and transverse acoustic instabilities. *Journal of Propulsion and Power*, 30:991–1004, 2014.

[18] Sebastian Karl. *Numerical Investigation of a Generic Scramjet Configuration*. PhD thesis, Technische Universität Dresden, 2011.

MODELLING FLAME RESPONSE OF COAXIAL LOX/GH2 ELEMENT TO HIGH FREQUENCY ACOUSTIC FORCING

[19] G. Lacaze and J.C. Oefelein. A non-premixed combustion model based on flame structure analysis at supercritical pressures. *Combustion and Flame*, 159:2087–2103, 2012.

[20] E.W. Lemmon and R.T. Jacobsen. Viscosity and thermal conductivity equations for nitrogen, oxygen, argon, and air. *International Journal of Thermophysics*, 25(1):21–69, 2004.

[21] A. Mack and V. Hannemann. Validation of the unstructured DLR TAU-code for hypersonic flows. In *Proceedings of the 32nd AIAA Fluid Dynamics Conference and Exhibit*, number AIAA-2002-3111, St. Louis, Missouri, 2002.

[22] Joseph C. Oefelein. Thermophysical Characteristics of Shear-coaxial LO_x-H_2 Flames at Supercritical Pressure. *Proceedings of the Combustion Institute*, 30:2929–2937, 2005.

[23] Joseph C. Oefelein. Mixing and Combustion of Cryogenic Oxygen-Hydrogen Shear-Coaxial Jet Flames at Supercritical Pressure. *Combustion Science and technology*, 178:229–252, 2006.

[24] M. Oschwald, J.J. Smith, R. Branam, J. Hussong, A. Schik, B. Chehroudi, and D. Talley. Injection of fluids into supercritical environments. *Combustion Science and Technology*, 178:49–100, 2006.

[25] Guillaume Ribert, Nan Zong, Vigor Yang, Laetitia Pons, Nasser Darabiha, and Sebastien Candel. Counterflow diffusion flames of general fluids: Oxygen/hydrogen mixtures. *Combustion and Flame*, 154(3):319 – 330, 2008.

[26] C.-C. Rossow. Extension of a compressible code toward the incompressible limit. *AIAA Journal*, 41(12):2379–2386, 2003.

[27] M. Schmid. *Thermoakustische Kopplungsmechanismen in Flüssigkeitsraketentriebwerken*. PhD thesis, Munich Technical University, 2014.

[28] D. Schwamborn, T. Gerhold, and V. Hannemann. *On the Validation of the DLR-TAU Code*, chapter 72, pages 426 – 433. Number ISBN 3-528-03122-0. New Results in Numerical and Experimental Fluid Mechanics, Notes on Numerical Fluid Mechanics, 1999.

[29] Dieter Schwamborn, Thomas Gerhold, and Ralf Heinrich. The DLR TAU-code: Recent Applications in Research and Industry. In P. Wesseling, E. Onate, and J. Périaux, editors, *European Conference on Computational Fluid Dynamics (ECCOMAS CFD)*, TU Delft, The Netherlands, September 5-8 2006.

[30] K.J. Shipley, W.E. Anderson, M.E. Harvazinski, and V. Sankaran. A computational study of transverse combustion instabilit mechanisms. In *AIAA Propulsion and Energy 2014*, 2014.

[31] P.R. Spalart and S.R. Allmaras. A one-equation turbulence model for aerodynamic flows. In *30th Aerospace Sciences Meeting and Exhibit, Aerospace Sciences Meetings*, number AIAA-92-0439, Reno,NV,U.S.A., 6-9 January 1992.

[32] A. Urbano, L. Selle, G. Staffelbach, B. Cuenot, T. Schmitt, S. Ducruix, and S. Candel. Exploration of combustion instability triggering using large eddy simulation of a multiple injector liquid rocket engine. *Combustion and Flame*, 169:129–140, 2016.

[33] Samuel Charles Leslie Webster. *Analysis of Pressure Dnymaics, Forced Excitation and Damping in a High Pressure LOX/H2 Combustor*. PhD thesis, RWTH Aachen University, 2016. DLR Forschungsbericht 2016-17.

[34] B. A. Younglove. Thermophysical properties of fluids. 1. argon, ethylene, parahydrogen, nitrogen, nitrogen trifluoride and oxygen. *Journal of Physical and Chemical Reference Data*, 11:Supplement No. 1, 1982.